AFRL-OSR-VA-TR-2013-0013

Quantum Ring Intersubband Detectors for Terahertz Detection at High Temperatures

Pallab Bhattacharya, Sishir Bhowmick, Guan Huang, Wei Guo, Chi-Sen Lee, Gamini Ariyawansa, A.G. Unil Perera

University of Michigan

April 2013
Final Report

DISTRIBUTION A: Approved for public release.

AIR FORCE RESEARCH LABORATORY
AF OFFICE OF SCIENTIFIC RESEARCH (AFOSR)
ARLINGTON, VIRGINIA 22203
AIR FORCE MATERIEL COMMAND

REPORT DOCUMENTATION PAGE

Form Approved OMB No. 0704-0188

1. REPORT DATE *(DD-MM-YYYY)*
10/17/2011

2. REPORT TYPE
Final Performance Report

3. DATES COVERED *(From - To)*
09/01/2009-08/31/2011

4. TITLE AND SUBTITLE
Quantum Ring Intersubband Detectors for Terahertz Detection at High Temperatures

5a. CONTRACT NUMBER
FA9550-09-C-0106

5b. GRANT NUMBER
FA9550-09-1-0635

5c. PROGRAM ELEMENT NUMBER

6. AUTHOR(S)
Pallab Bhattacharya, Sishir Bhowmick, Guan Huang, Wei Guo, Chi-Sen Lee, Gamini Ariyawansa, A.G. Unil Perera

5d. PROJECT NUMBER

5e. TASK NUMBER

5f. WORK UNIT NUMBER

7. PERFORMING ORGANIZATION NAME(S) AND ADDRESS(ES)
University of Michigan
503 Thompson Street
Ann Arbor, MI 48109-1340

8. PERFORMING ORGANIZATION REPORT NUMBER

9. SPONSORING / MONITORING AGENCY NAME(S) AND ADDRESS(ES)
Air Force Office of Scientific Research
801 North Randolph Street, Room 732
Arlington, VA 22203-1977

10. SPONSOR/MONITOR'S ACRONYM(S)

11. SPONSOR/MONITOR'S REPORT NUMBER(S)
AFRL-OSR-VA-TR-2013-0013

12. DISTRIBUTION / AVAILABILITY STATEMENT

Distribution A: Approved for public release

13. SUPPLEMENTARY NOTES

14. ABSTRACT
The research was focused on the development of quantum ring intersubband detectors for the 1-3 THz range and demonstration of raster scan imaging with these detectors. Molecular beam epitaxy of relatively small InAs/GaAs quantum dots and their subsequent transformation to quantum rings by post-epitaxy thermal annealing was investigated. Photoconductive detectors with multiple quantum ring layers in the active region and a single barrier at the end of the heterostructure exhibited very low dark current density. The rings have a single bound state and emission of photoexcited carriers gives rise to a spectral response peaking at 1.82 THz (165 μm) at 5.2 K. The peak responsivity is 25 A/W. Raster scan imaging was also investigated with the detectors where a seven segment display and an incandescent light bulb filament were imaged in the 1-3 THz range.

15. SUBJECT TERMS

16. SECURITY CLASSIFICATION OF: a. REPORT	b. ABSTRACT	c. THIS PAGE	17. LIMITATION OF ABSTRACT	18. NUMBER OF PAGES	19a. NAME OF RESPONSIBLE PERSON
u	u	u	sar	6	**19b. TELEPHONE NUMBER** *(include area code)*

Accomplishments:

The most significant accomplishment of this project was (i) the demonstration of quantum ring intersubband detectors in the 1-3 THz range with very high responsivity and specific detectivity; (ii) the demonstation of a raster scan imaging with those detectors. A more detailed description of these accomplishments is as follows:

1. Quantum Ring Intersubband Detectors for the 1-3 THz Range:

The objective of the project was to investigate the design and characteristics of quantum ring intersubband detectors for the 1-3 THz range and also to demonstrate imaging with those detectors. We have investigated the characteristics of small quantum rings grown by molecular beam epitaxy (MBE) and of intersublevel THz photoconductive detectors with quantum ring active regions. It is found that the quantum ring intersublevel detectors (QRIDs) exhibit very low dark current and strong response in the 1-3 THz range, with the peak response measured at 1.82 THz (165 µm) in the temperature range of 5-10 K. This detection peak is characterized by a peak responsivity of 25 A/W; specific detectivity of 1×10^{16} Jones and response time ~300 ps [1]. These characteristics compare very favorably with those of bolometers.

In order to get an estimate of the size of the QRs in which the intersublevel spacing would be in the 1-3 THz range, we have performed calculations using a simplified model. From atomic force microscopy (AFM) images such as one shown in Fig. 1(a), it is evident that the rings have a height in the range of 1.2-1.5 nm and inner and outer radii of 25 and 40 nm, respectively. Carrier confinement in the rings primarily results from their width and height. We have therefore, approximated the ring by a quantum wire of equal width and height and solved the three dimensional (3-D) Schrodinger equation using appropriate boundary conditions. The thickness of the surrounding GaAs layer is assumed to be large enough along the nanowire height and width, such that the wavefunction can be assumed to be zero at the boundaries, while periodic boundary conditions exist along the length of the nanowire. The eigen energies of the matrix Hamiltonian are then calculated. With the dimensions considered, there is only one bound state in the potential well and Fig. 1(b) shows the energy positions of this state, which is also the ground state. It is evident that for QR height of 1.2-1.5 nm and width of 15 nm, the transition energy from the ground state to the continuum in the ring corresponds to the frequency range of 1-3THz. It is important to note that the single confined state in the quantum ring can be obtained only if they are made small. It may also be noted that we have used a simplified model for this calculation. In reality, the picture is more complex due to the actual shape of the ring and wavefunction overlap.

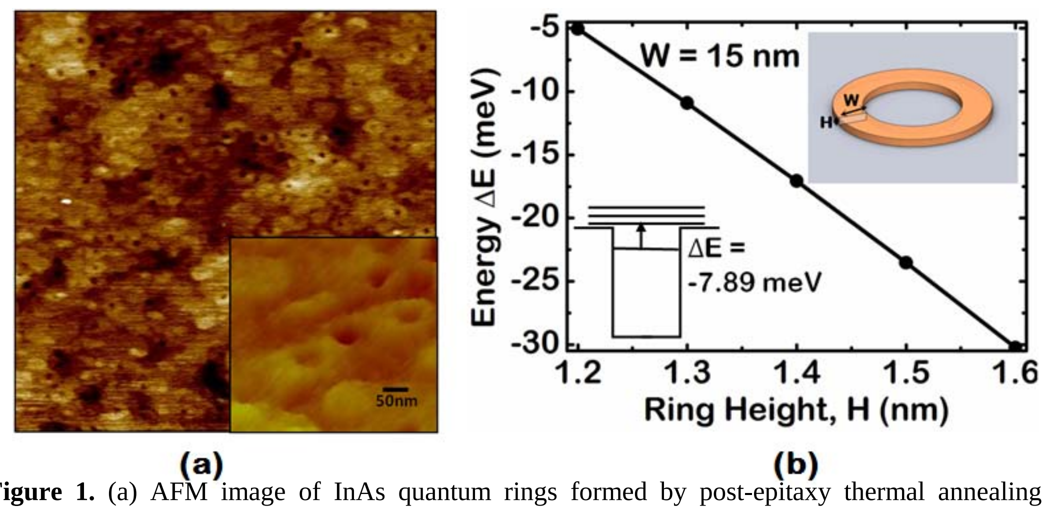

Figure 1. (a) AFM image of InAs quantum rings formed by post-epitaxy thermal annealing of quantum dots. Inset shows a magnified image and dimensions; (b) calculated ground state energy in the quantum ring as a function of ring height for ring width W = 15 nm. Insets shows the schematic of the quantum ring and calculated bound state in a quantum ring with W = 15 nm and H = 1.25 nm. The transition energy of 7.89 meV corresponds to 1.91 THz.

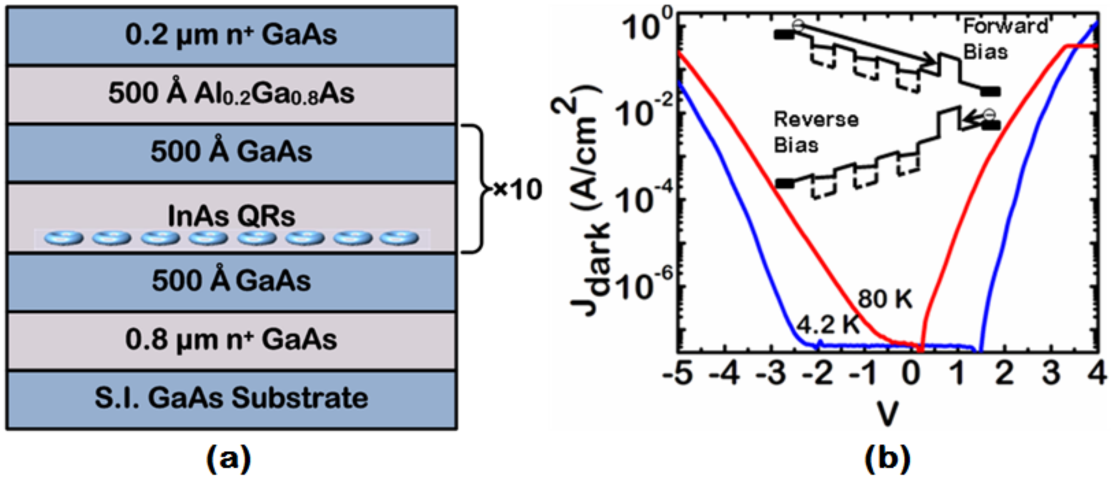

Figure 2. (a) Heterostructure schematic of QRID grown by MBE. It has 10 layers of InAs quantum rings in the active region and a single $Al_{0.2}Ga_{0.8}As$ barrier at the end; (b) dark current characteristics at two different temperatures (4.2 K and 80 K). Inset shows the conduction band profiles in the active region for forward and reverse bias.

The quantum ring ensembles and photoconductive detectors containing multiple QR layers were grown by MBE on semi-insulating (001) GaAs substrates. The growth parameters for the initial InAs quantum dots and the anneal conditions to convert them to quantum rings were investigated and carefully tuned to produce the desired smaller size of these nanostructures. For these experiments, a 0.8 μm GaAs buffer layer was first grown at 600°C. The substrate temperature was then lowered to 530°C and 2.1 monolayers of InAs was deposited at a rate of 0.08 monolayer/sec. Self-organized quantum dots were formed following growth of 1.8 monolayers of InAs wetting layer. A 10Å AlAs cap layer was grown on the InAs islands at 530°C. Growth was interrupted and the capped islands were annealed at 580°C for 30 sec under an As_2 flux to form quantum rings. The function of the AlAs layer was to reduce the surface mobility of group III atoms on the AlAs surface, since AlAs has a higher bonding strength than GaAs. Consequently, the ring shape is better preserved during the annealing process. Under these growth conditions, small quantum rings as shown in the AFM image of Fig. 1(a) are obtained. The detector heterostructure, grown with 10 QR layers separated by 50 nm GaAs barriers, is shown in Fig. 2(a). A single $Al_{0.2}Ga_{0.8}As$ barrier is inserted at the end. In quantum dot infrared photodetectors (QDIPs), the insertion of a single barrier layer has been very effective in reducing the dark current without substantially affecting the photocurrent [2]. The band profiles of the heterostructure for forward and reverse bias are shown in the inset of Fig. 2(b). Mesa shaped devices for top illumination were fabricated by photolithography, wet chemical etching and n-contact metallization. The ring-shaped top contact has an inner radius of 300 μm, which defines the illumination area.

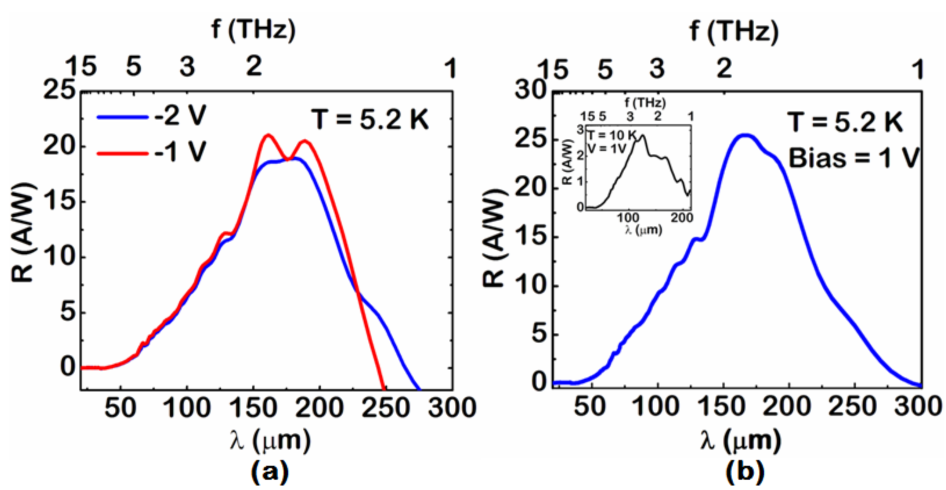

Figure 3. Measured spectral responsivity of QRID for (a) different reverse biases measured at 5.2 K, and (b) 1V bias measured at 5.2 K. The inset to (b) shows the responsivity at 10 K under

The QRIDs were characterized at cryogenic temperatures by dark current-voltage (I-V), spectral response and noise measurements. The processed detectors were mounted on chip carriers with silver epoxy and individual devices were wire bonded to separate chip carrier leads. The mounted devices were inserted in a variable temperature liquid He cryostat for I-V measurements, which was done using a Keithley 2400 Source Meter. In order to determine the spectral responsivity of the detectors, the spectral response of the device under test and a Si composite bolometer with a known sensitivity were measured with a Perkin Elmer System 2000 Fourier Transform Infrared (FTIR) spectrometer. The two spectra were recorded with the same combination of optical windows, beam-splitter, and filters, so that the optical path is identical. A glow-bar was used as the radiation source. In order to confirm that the detection is not due to short wavelength (< 62 μm) radiation, as in an optical pumping situation, a 62 μm cut-on filter was placed in front of the detector and the same detector response (but with reduced intensity due to the low transmission coefficient of the filter) was obtained. The voltage responsivity in V/W of the detectors was calculated by, $R = GSI_d/I_b$, where I_d is the raw detector spectrum, I_b is the bolometer raw spectrum, S is the bolometer sensitivity, and G is a geometrical factor which corrects for differences in the radiation-incident-area of the detector and the bolometer. To obtain the current responsivity in A/W, the voltage responsivity was divided by the effective resistance, which is the parallel combination of the load resistance R_l and the detector dynamic resistance R_d (= dV/dI).The specific detectivity of the detectors at different temperatures and applied biases was obtained from, $D^* = R_p\sqrt{A}/\sqrt{S_i}$ where R_p is the measured peak responsivity, S_i is the noise current density, and A is the illuminated area of the detector. The noise current density was measured with a dual channel Fast Fourier Transform (FFT) signal analyzer and a SR570 low noise current pre-amplifier.

The measured dark current densities at 4.2 K and 80 K are shown in Fig. 2(b). The asymmetry in the I-V curves is due to the asymmetric structure of the device and can be understood in terms of the conduction band profiles shown in the inset. It may be noted that the dark current densities are extremely low; at T = 4.2 K, J = 10^{-8} A/cm^2 and 10^{-6} A/cm^2 for bias of -2V and +2V, respectively. At T = 80 K, J = 10^{-5} A/cm^2 and 10^{-3} A/cm^2 for bias of -2V and +2V, respectively.

The calibrated spectral response of the QRIDs at different biases and temperatures are shown in Figs. 3(a) and (b). There are several important points to be noted in the data. The responsivity peak at 1.82 THz (165 μm) corresponds to an energy of 7.52 meV, which agrees with the calculated ground state-to-continuum transition energy shown in Fig. 1(b) for the ring height of 1.25 nm. The observed high peak value of the responsivity R_p ~ 20 or 25 A/W, depending on bias polarity is due to the fact that the number of photons per 1 W of power at long wavelengths is higher compared to that in short wavelengths. The total quantum efficiencies (internal quantum efficiency × gain) are ~ 15 and 19% at -1 and 1 V bias values, respectively. The $Al_{0.2}Ga_{0.8}As$ barrier layer with a height of 150 meV (assumed to be equal to the conduction band offset), does not seem to impede the transport and collection of photogenerated carriers under forward bias operation. The peak responsivity is larger under the forward bias than under the same amount of reverse bias (1V). It may be noted that the trend of the dark current is also the same. We believe that the dark current contributes to the filling of bound states in the quantum ring with electrons which eventually contribute to the photocurrent and responsivity. Hence, the trend in peak responsivity follows that of the dark current for opposite bias polarities. From Fig. 3(b) it is evident that the responsivity decreases sharply with increase of temperature from 5.2 K to 10 K. In fact, at 12 K, the spectral response is too weak to measure. Due to the small energy difference between the bound state and the continuum in the quantum rings, any increase in temperature leads to emptying of electrons from the bound states to the states in the continuum. This also explains the shift of the responsivity peak to a higher energy (by 2.6 meV) when the measurement temperature is increased from 5.2 K to 10 K (Fig. 3(b)). The values of specific detectivity D^*, at a bias of 1V, derived from the measured peak responsivity and noise current, are 1×10^{16} Jones and 3×10^{15} Jones at 5.2 K and 10 K respectively.

2. Raster Scan Imaging with Quantum Ring Intersubband Detectors:

We demonstrated imaging of an incandescent light bulb filament and of a seven segment display using the raster scan technique and detection with a single terahertz quantum ring intersubband detector (QRID) [3]. Raster scanning of the objects was accomplished with a Proseries-II scanner which has two silver plated mirrors (highly reflective in the long wavelength and THz ranges) servoactuated by galvanometers. The drive circuitry of the galvanometer was interfaced with a computer in order to have a precise control of the motion of the mirrors. The raster scan motion of the mirrors directs the radiation on to the QRID for detection. The QRID was housed in a cryostat with a window for signal access and was held at a temperature of 5.2 K. The voltage variation across the detector was amplified using lock-in techniques. Each output voltage of the lock-in amplifier, which corresponds to a specific point on the object, was acquired and stored in a computer using data acquisition software. The schematic of the measurement system is very similar to our previous demonstration of imaging with quantum dot intersubband detector [4] and is schematically shown in Fig. 4. The resolution of the image is determined by the incremental motion of the scanning mirrors and the time constant of the lock-in amplifier. In other words, it depends on the minimum rotation step of the mirrors as well as the distance of the object from the mirror. Based on the images obtained in the course of present work, we estimate the resolution of our raster scanning is 0.1 mm.

Ideally, THz detectors can image an object which is warm or hot. However in this experiment we choose to image an incandescent light bulb filament and a seven segment display because of the size constraints imposed by the scanning mirrors. The objects were placed 10 cm away from the mirrors and directly in front of and perpendicular to the QRID. A filter was placed between the mirrors and the detector to filter out short wavelength radiation. Figure 5(a) shows the image of the incandescent light bulb filament of dimension 5 mm × 0.2 mm. Figure 5(b) shows the image of a seven segment display of the digit “2”. The dimension of the display is 10 mm × 5 mm. The lack of contrast in the images is mainly due to the conductivity saturation of the detector caused by background radiation from the objects. The large peak responsivity of 13.5 A/W, specific detectivity D^* of 1×10^{16} Jones and a total quantum efficiency of 15% of the QRID, as mentioned earlier, are very favorable characteristics. However, they also imply that a minimal background radiation can excite all the electrons from the bound state in the quantum rings to the continuum level and the conductivity of the device saturates. As a result, the differential conductivity of the device decreases, which in turn degrades the contrast in the reconstructed images. For the particular QRID device used in this experiment, the internal quantum efficiency is 34% and the carrier effective life time is $\sim5\times10^{-10}$ sec [5]. Therefore, for a photon flux density of 5.8×10^{18} cm^{-2}, which corresponds to an optical power density of 7 mW / cm^2 for a 165 μm wavelength photon, all the bound state electrons in the QRs are excited to the continuum levels and the conductivity of the device saturates. This problem can be minimized by using an array of devices interconnected in parallel, using appropriate optics and also by applying signal processing techniques. It may be noted that our present imaging device has a single bound state ~7 meV below the continuum level. Since the energy difference between the bound state and the continuum level is extremely small, any increase in temperature beyond 10 K results in emptying the bound states and loss of detector operation. The temperature of operation in the 1-3 THz range can be improved with a device having a deeper ground state and an excited state ~7 meV below the continuum level. In this case, it is

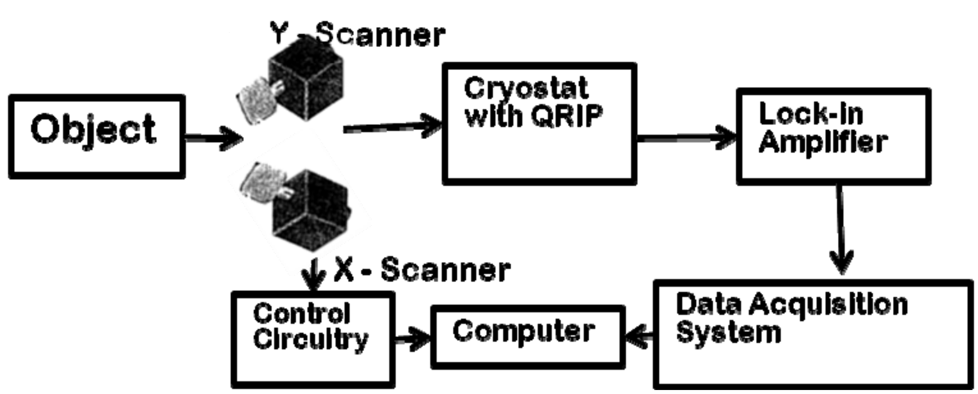

Figure 4. Schematic measurement setup system.

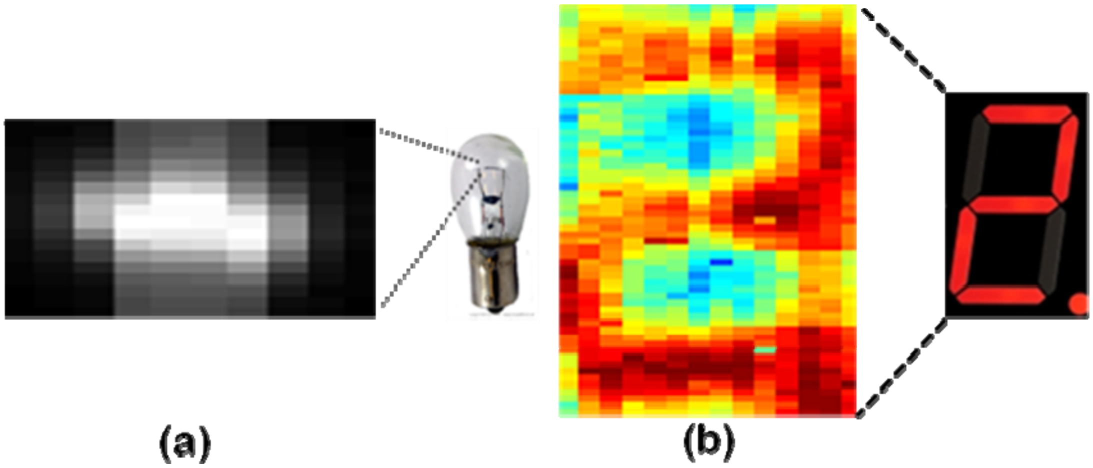

Figure 5. Raster scan images obtained using QRID: (a) an incandescent light bulb; b) seven segment display of the digit “2”.

expected that at higher temperature the carriers will be thermally excited from the ground states to the excited states and then in the presence of THz radiation, they will be photo-excited to the continuum level. Based on the energy level calculation method discussed by us in a previous publication [3], we find that an InAs quantum ring of width 18 nm and height of 1.5 nm has energy levels 27.7 and 8.9 meV below the continuum level which would be ideal for THz detection in the 1-3 THz rage at higher temperature (~80-100K). Experiments are in progress to improve the temperature of operation as well as the imaging properties of the device.

References:

1. C.H. Lin, H.S. Lin, C.C. Huang, S.K. Su, S.D. Lin, K.W. Sun, C.P. Lee, Y.K. Liu, M.D. Yang, and J.L. Shen, *Appl. Phys. Lett.* **94**, 183101 (2009).
2. A.D. Stiff, S. Krisna, P. Bhattacharya, and S.W. Kennerly, *IEEE Journal of Quantum Electronics*, **37** (11), 1412 (2001).
3. S. Bhowmick, G. Huang, W. Guo, C.S. Lee, P. Bhattacharya, G. Ariyawansa, and A.G.U. Perera, “High-performance quantum ring detector for the 1–3 terahertz range”, *Appl. Phys. Lett*. Vol. 96**,** pp. 231103, 2010.
4. A.D. Stiff, S. Chakrabarti, S. Pradhan, B. Kochman, and P. Bhattacharya,” Raster-scan imaging with normal-incidence, midinfrared InAs/GaAs quantum dot infrared photodetectors”, *Appl. Phys. Lett.*, vol. 80, no. 18**,** pp. 3265- 3267, May 2002.
5. B. Kochman, A.D. Stiff-Roberts, S. Chakrabarti, J. D. Phillips, S. Krishna, J. Singh, and P. Bhattacharya, “Absorption, Carrier Lifetime, and Gain in InAs–GaAs Quantum-Dot Infrared Photodetectors”, *IEEE Journal of Quantum Electronics*, vol. 39, no. 03, pp. 459-467, Mar. 2003.

Group Publications during the grant period:

Journals:

1. S. Bhowmick, G. Huang, W. Guo, C.S. Lee, P. Bhattacharya, G. Ariyawansa, and A.G.U. Perera, “High-performance quantum ring detector for the 1–3 terahertz range”, *Appl. Phys. Lett*. Vol. 96**,** pp. 231103, 2010.

Conferences:

1. S. Bhowmick, G. Huang, W. Guo, C.S. Lee, P. Bhattacharya, G. Ariyawansa, and A.G.U. Perera, “A Quantum Ring Detector for the 1-3 Terahertz Range with Very High Responsivity and Specific Detectivity”, Device Research Conference 2010, University of Notre Dame, Indiana.